Environmental Science & Technology

pubs.acs.org/est

Article

Total Bioaerosol Detection by a Succinimidyl-Ester-Functionalized Plasmonic Biosensor To Reveal Different Characteristics at Three Locations in Switzerland

Guangyu Qiu, Yang Yue, Jiukai Tang, Yi-Bo Zhao, and Jing Wang*

Cite This: https://dx.doi.org/10.1021/acs.est.9b05184

Read Online

ACCESS | Metrics & More | Article Recommendations | Supporting Information

ABSTRACT: Bioaerosols consisting of biologically originated airborne particles such as microbes, metabolites, toxins, and fragments of microorganisms are present ubiquitously in our living environment. The international interests in bioaerosols have rapidly increased because of their many potential health effects. Thus, accurate and fast detection of total bioaerosols in different environments has become an important task for safeguarding against biological threats and broadening the pool of bioaerosol knowledge. To quickly evaluate the total bioaerosol concentration, we developed a localized surface plasmon resonance biosensor based on succinimidyl-ester-functionalized gold nanoislands (SEF−AuNIs) for quantitative bioaerosol detection. The detection limit of our proposed SEF−AuNI sensors for model bacteria *Escherichia coli* and *Bacillus subtilis* can go to 0.5119 and 1.69 cells/mL, respectively. To demonstrate the capability of this bioaerosol sensing technique, we tested aerosol samples collected from Bern (urban station), Basel (suburban station), and Rigi mountain (rural and high altitude station) in Switzerland and further investigated the correlation with endotoxin and PM10. The results substantiated that our SEF−AuNI sensors could be a reliable candidate for total bioaerosol detection and air quality assessment.

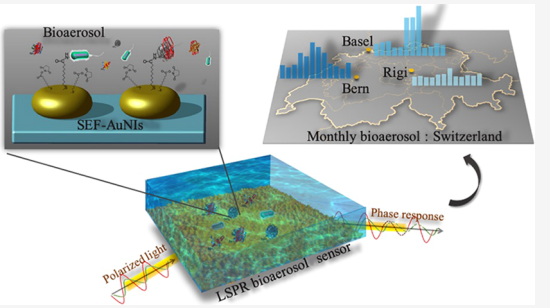

INTRODUCTION

Bioaerosols refer to the airborne particles of biological origin.[1,2] Plants, soil, water, and animals as sources of bioaerosols can make them present pervasively in our daily lives.[1] The interest in bioaerosols has dramatically increased over the past few decades, to understand their emission, distribution, and significant human health impacts.[3−6] It has been recognized that exposures to biological agents are associated with a wide range of adverse health effects and have direct influences on our daily lives.[7,8] The health hazards associated with bioaerosols range from mild reactions to much more severe reactions, such as cancer and death caused by airborne pathogens.[9,10] Three major categories of diseases associated with bioaerosol exposure can be identified: infectious disease, respiratory disease, and cancer.[11] Generally, bioaerosols consist of both viable and nonviable components including fungi, bacteria, viruses, and pollens. Because of the difficulties of preserving the biological activity of bioaerosols during sampling, the bioaerosol concentration and their health effects are easily underestimated when using the culture- and molecular-based methods. Thus, accurate and fast detection of total bioaerosols which contain both viable and nonviable airborne microorganisms is crucial for a better understanding of their population, distribution, and health impacts.

Over the past decade, there has been an increasing interest in developing specific technologies and methods that can detect and characterize the population of bioaerosols.[12−15] Bioaerosols can be quantified by culturing and nonculturing-based methods. The conventional culture-based methods can provide information on speciation of the viable bioaerosols such as airborne fungi and bacteria.[16] Unfortunately, it is difficult to discriminate against different bacteria because the colonies might look similar. Furthermore, only a small proportion of the total bioaerosols presented in our living environments are culturable, which leads to an underestimation of the total airborne microorganism concentration. It has been proven that the nonculturable bioaerosols, for example, viruses and archaea can also cause allergies or health effects similar to viable microorganisms.[17] Detection techniques based on molecular biology provide another approach for bioaerosol monitoring.[18,19] One of the most commonly used molecular methods in microbial studies is based on the detection of genetic materials of organisms present in a given sample, such as the polymerase chain reaction (PCR).[20,21] However, concentrating and retrieving the biological materials from aerosol samples prior to analyses are necessary.

Received: August 28, 2019
Revised: January 6, 2020
Accepted: January 7, 2020
Published: January 7, 2020

Moreover, it is indispensable to select the precise genomic regions to amplify for obtaining the most accurate information about the microbial content.[18] For example, the conserved 16S rRNA prokaryotic gene can be used for bacteria detection. However, viral detection has been challenging due to the lack of universal and conserved markers.[22] The sensors based on laser-induced fluorescence can be employed for online quantification of the total bioaerosol concentration.[23,24] The relevant microorganisms containing molecules such as aromatic amino acids and reduced nicotinamide adenine dinucleotide can be quantified based on the characteristic fluorescence when excited by UV radiation. The fluorescence-based detection system is the most common online technique for bioaerosol detection and has been commercially used in some total bioaerosols monitors, such as wideband-integrated bioaerosol sensor (WIBS, Droplet Measurement Technologies, Longmont, USA), Ultraviolet Aerodynamic Particle Sizer (TSI Inc., St. Paul, MN, USA), biological-agent warning sensors (Battelle, Columbus, Ohio, USA), and BioScout (ENVI BioScout, Environics Ltd., Mikkeli, Finland).[15,25] Other devices based on the analysis of holographic images, light scattering, and fluorescence signals are optimized for the identification of pollen at the taxa level, such as Swisens Poleno (Swisens AG, Switzerland) and Raped-E (Plair S.A., Switzerland).[26−28] Generally, the species-level identification with the laser-induced fluorescence method is relatively difficult, as the related classes of bioaerosols may have similar spectra.[15] Thus, this technique is still primarily used for the quantitative monitoring of total bioaerosols. However, many natural harmless particles including nonbiological particles also fluoresce, which may cause an unacceptable false-positive signal. Similarly, the atomic emission spectroscopy (AES) refer to the elementary analysis of aerosol samples by excitation (e.g., thermal or plasma) and detection of the emitted radiation.[29,30] The organic elements (e.g., C, H, O, and N) and mineral elements (e.g., Mg, Na, Fe, K, and Ca) can be used as nonspecific markers of bioaerosol by AES. However, the AES method is also significantly influenced by the optical dispersion and particle background. Furthermore, the bioaerosol species were difficult to be discerned by the AES method.[31]

Localized surface plasmon resonance (LSPR) is a strong electromagnetic near-field coupling effect associated with noble-metal nanostructures.[32] The excited plasmonic fields can directly provide signals for the local changes of molecular biophysical properties such as refractive index (RI) and molecular weight in a label-free manner. Owing to the enhanced plasmonic field in the vicinity of the nanostructures, LSPR sensing systems demonstrated high sensitivity to local variation.[33] Thus, LSPR is an ideal candidate for real-time and label-free detection of micro- and nanoscale analytes. Previous studies have shown that conventional surface plasmon resonance (SPR) sensors allow rapid and precise detection of airborne pathogens based on immunoreaction with the antibody.[34,35] Similar to other immunoassay-based biosensing systems, these SPR sensors mainly targeted the analyte of a single type, such as proteins, small organics, bacteria, viruses via interactions between specific ligands (e.g., antibody−antigen).[36,37] For example, plasmonic-based immunosensors coupled with a specific antigen−antibody reaction has been proposed by Usachev et al. in 2014 for fast detection of bioaerosols of a single type, that is, the surrogate MS2 bacteriophage.[34] Similar to the enzyme-linked immunosorbent assay method, the plasmonic antibody-based immunosensors have the benefit of providing information on bioaerosol species. Natural bioaerosols represent a highly diverse group, and different species possess various toxicities. Obtaining information on the species of the detected bioaerosol is clearly beneficial; however, just detecting bioaerosols of a single type is not enough to meet the needs of air quality assessment. In fact, it has been realized that exposure to a complex mixture of toxins, allergens, and a wide range of different bioaerosols has to be considered in a rapid-response risk assessment.[8] Other than the pathogenic bioaerosols, the total bioaerosols including the nonpathogenic part should also be evaluated as it can induce respiratory symptoms as well.[11,38] Thus, fast, label-free, and reliable detection of total bioaerosols will be an important basis for a better understanding of bioaerosol behaviors and impacts. In this work, we developed a precise LSPR sensing system which can rapidly quantify the total bioaerosols by capturing microorganisms with succinimidyl ester-functionalized gold nanoislands (SEF−AuNIs) (Figure S1). The synthetic nanoislands were employed as a powerful and cost-effective sensing matrix due to the formation of strong plasmonic hot spots within the nanogaps.[39] The AuNI sensors can be readily nanofabricated on large areas and subsequently surface-functionalized with thiolate and succinimide esters. The exposed amino groups from bioaerosols can be covalently captured and detected by the SEF−AuNI sensors. For example, the protein shell of the virus, also known as the capsid, consists of oligomeric structural subunits.[40] This oligomeric protein contains amino groups which can be captured by the SEF−AuNIs sensors. Similarly, the functional or structural proteins from the fungal cell wall, bacterial outer membrane, pollen exine, and their fragments all contain amino groups.[41−43] By capturing the amino groups from these bioaerosols, the SEF−AuNIs sensors can achieve quantitative detection of total bioaerosols in a label-free scheme. Therefore, it can be used for label-free detection of all species of airborne microorganisms even without a premeasured library in contrast to previous studies. To the best of our knowledge, this is the first study to characterize the total bioaerosols with interferometric LSPR biosensors and to apply it on studying real-world environmental samples.

MATERIALS AND METHODS

LSPR Sensor Preparation. The LSPR sensor chip with annealed AuNIs was synthesized by the thermal dewetting method.[44] Specifically, an ultrathin gold film with 5.2 nm nominal thickness was initially deposited on the cleaned BK7 glass slides by magnetron sputtering. Then, the Au-coated substrate was thermally annealed at 550 °C for 3 h in the air to form the nanoislands in a self-assembly manner. Then the AuNIs chips were subsequently mounted into the common-path white light interferometric sensing system for differential phase detection of binding events.

Environmental Sample Collection and Preparation. The aerosol samples were collected at three Swiss National Air Pollution Monitoring Network (NABEL) stations in Bern (Bollwerk, urban), Basel (Binningen, suburban), and Rigi (Seebodenalp, rural) in 2017. The sampling station in Bern was located on a traffic-intensive roadside with approximately 20,000 vehicles passing by every day. The sampling point was 4 m away from the road, and there were many high-rise buildings on both sides of the road. The sampling station in the suburban of Basel was located in a quiet park-like place, with a

https://dx.doi.org/10.1021/acs.est.9b05184
Environ. Sci. Technol. XXXX, XXX, XXX−XXX

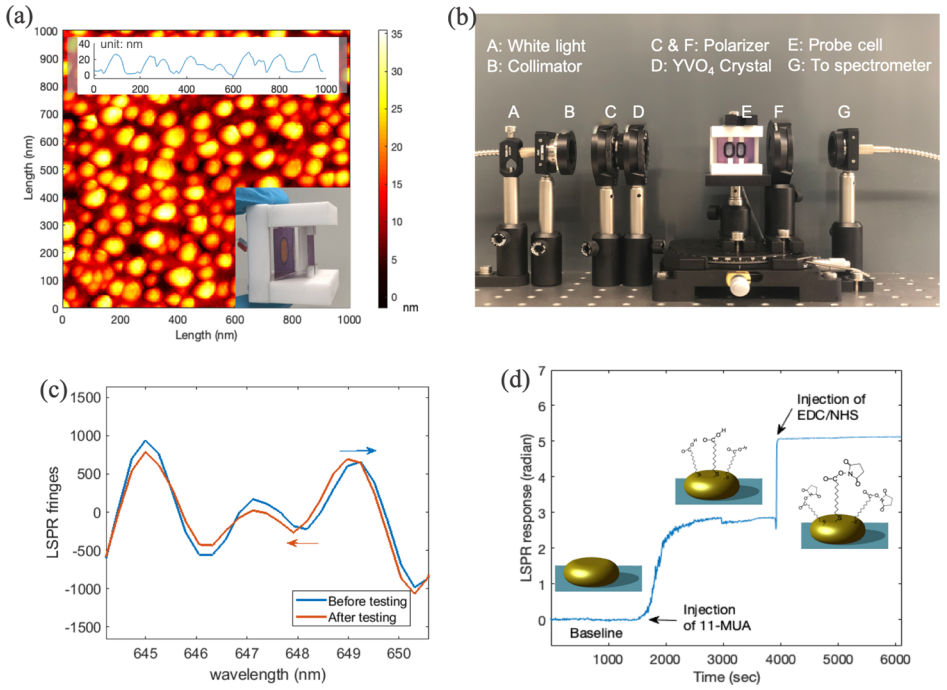

Figure 1. (a) Characterization of AuNIs with tapping-mode AFM and (inset) an image of the sensing probe cell and surface morphology profile. (b) Common-path LSPR phase sensing system. (c) Interferometric fringes before and after the sensing test showed a phase change at evanescent sensing wavelength, that is, about 647.5 nm. (d) In situ phase sensing response of surface functionalization, including the anchor 11-MUA and activator EDC/NHS.

high green-cover rate. The monitoring station of Rigi-Seebodenalp was located on the Rigi mountain above 1000 m.a.s.l. and represented a rural and high-altitude environment. The aerosols were collected on quartz fiber filters (150 mm in diameter) by using high-volume samplers (DHA-80, Digitel). The sampling flow rate was 500 L/min, and the total air sampling volume was approximately 642.9 m^3/filter. The daily samples were stored at −20 °C after sampling. With a puncher, the 490 mm^2 section was taken from each filter and daily particulate matter (PM) samples from each month were pooled together to represent the respective month. All the filters from each month were deposited into 60 mL phosphate-buffered saline (PBS, pH 7.4) and shaken with a speed of 1000 rpm for 30 min. Then, the sample was transferred to a tube and centrifuged at 3500 rpm to remove the filter and fiber fragments. The supernatants were stored at −20 °C until the endotoxin and LSPR analysis.

Endotoxin Testing. For the endotoxin studies, all environmental samples were analyzed using limulus amebocyte lysate (LAL) (Associates of Cape Cod Inc.) gel-clot method, and the concentrations were reported as units (EU) referring to standard endotoxin and lipopolysaccharides (LPS) from *Escherichia coli*. In the test, equal volume of samples and LAL reagent were incubated at 37 °C and reacted with the gel-clot product. The absorption of 405 nm light was recorded every 30 s for 90 min during the measurement. The detection limit for endotoxin was 0.005 EU/mL. Spike control, positive control, negative control, and blank samples were also included to ensure the test quality.

Surface Functionalization and LSPR Bioaerosol Detection. The surface functionalization of the AuNI chip included two processes: the chemical immobilization of thiolate ligands and the activation of the carboxyl group. The thiolate ligands, that is, 11-mercaptoundecanoic acid (11-MUA) were initially immobilized on the AuNI surface by forming the Au−S bond as shown in Figure S1b. Subsequently, the 2-(*n*-morpholino)ethane sulfonic acid (Sigma-Aldrich) activation solution prepared by mixing equal volume (500 μL) of 0.4 M 1-ethyl-3-(3-dimethylaminopropyl)carbodiimide (EDC, Sigma-Aldrich) and 0.15 M *N*-hydroxy-succinimide (NHS, Sigma-Aldrich) was added on the chip to activate the carboxyl group. The synthetic succinimidyl ester was susceptible to the nucleophilic attack by an amine group, leading to the formation of an amide bond linking the bioaerosols to the functionalized AuNIs. The prepared PM samples were diluted 1000 times just before the LSPR detection. The detailed surface functionalization and detection procedures are provided in Figure S1.

Atomic Force Microscopic Investigation and Surface-Enhanced Raman Scattering Studies. The AuNI sensing chips were studied with tapping mode atomic force microscopy (AFM) for visualizing the size and distribution of nanoislands. Moreover, the 11-MUA-functionalized AuNIs (MUA@AuNIs), SEF−AuNIs, and bioaerosols were characterized with surface-enhanced Raman scattering (SERS) by using a Horiba confocal Raman microscope with a 100× objective, 785 nm laser of 1 mW incident power, and 20 s acquisition time. SERS streamline mapping of a selected area of 400 μm^2 on a bioaerosol-bound SEF−AuNIs sample was performed with a 50× objective.

RESULTS AND DISCUSSION

Surface Functionalization of AuNIs. For AuNI fabrication, the as-deposited gold nanofilm was thermally annealed at 550 °C, which modified the nanofilm to randomly distributed nanoislands as shown in Figure 1a.[45] The optimal AuNI chip with an average nanoisland size of 40.2 nm (Figure S2) was subsequently mounted into the common-path

https://dx.doi.org/10.1021/acs.est.9b05184
Environ. Sci. Technol. XXXX, XXX, XXX−XXX

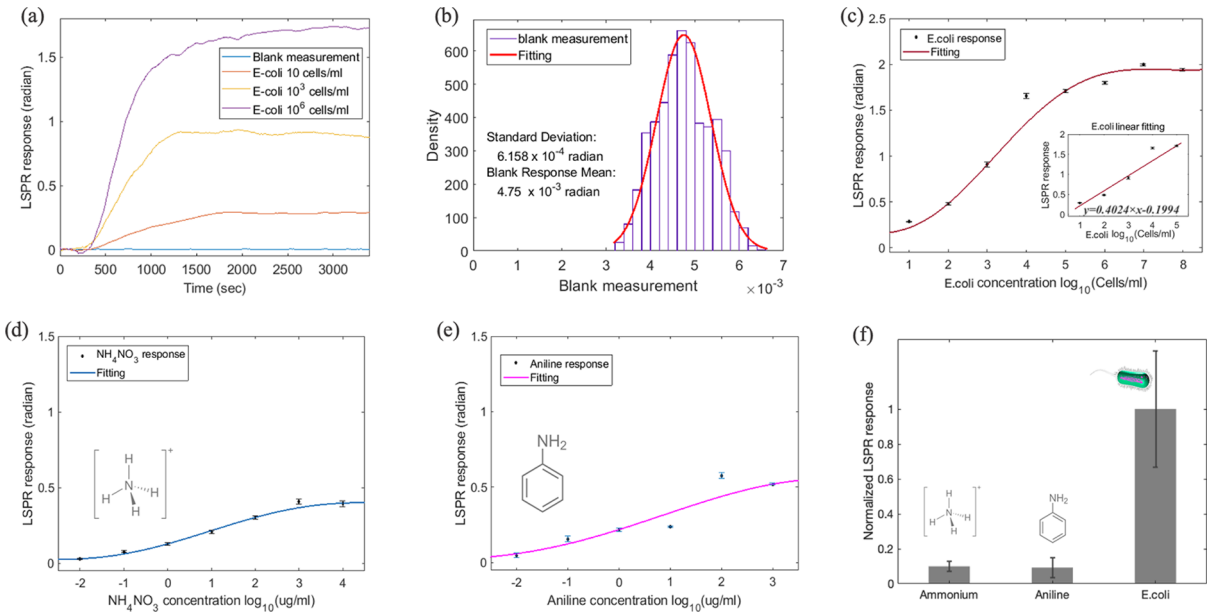

Figure 2. (a) Phase sensorgram of *E. coli* of various concentrations in PBS buffer, (b) signal distribution and Gaussian fitting of blank measurements. Logarithmic response curve of (c) *E. coli* with the linear regression inset, (d) ammonia ions, and (e) aniline. (f) LSPR sensing comparison of *E. coli*, ammonium ions, and aniline, which represented the bioaerosols, inorganic ammonium, and organic amine, respectively.

interferometric sensing system (Figure 1b) for differential phase detection. The interferometric LSPR system and differential phase interference fringes are given in Figures 1c and S3. It is worth noting that the interferometric sensing system can efficiently measure the plasmonic phase changes based on retrieving interferometric fringe with windowed Fourier transform methods and provide high sensitivity for bioaerosol detection.[46]

The sulfhydryl group of 11-MUA reacted with AuNIs by forming a strong covalent Au−S bond and produced significant response at 3.04 rad (Figure 1d), which could be used for in situ monitoring of surface functionalization. The MUA@AuNIs were subsequently activated by a freshly prepared mixture of EDC/NHS and induced a further phase increase by about 2.056 rad. Overall, the net LSPR response due to the ligand immobilization and activation was found to be 5.096 rad. Hereafter, the active succinimidyl ester was able to react with an amino group, leading to the formation of an amide bond when detecting bioaerosols.

SEF−AuNI Sensing Calibration. The sensing characteristics of the SEF−AuNI sensors were initially determined by detecting *E. coli* solutions of different concentrations ranging from 10 to 10^8 cells/mL. The blank sample (PBS buffer) without *E. coli* was used as the reference for evaluating the system stability and limit of detection (LOD). As shown in the real-time sensorgram (Figure 2a), the standard *E. coli* samples with three different concentrations, that is, 10, 1000, and 10^6 cells/mL produced continuous responses when captured by the SEF−AuNIs sensors. Generally, the interferometric fringes (Figure S3) were recorded every 2 s and the differential phase was calculated subsequently. When the blank PBS buffer flowed through the sensing chamber, the LSPR phase response of SEF−AuNIs remained stable at 4.75×10^{-3} rad with the standard deviation of 6.158×10^{-4} rad as shown in Figure 2b. Subsequently, the LSPR phase response was found to be 0.29 rad when detecting the standard *E. coli* sample of 10 cells/mL. The phase response increased to 0.87 and 1.78 rad when detecting the concentration of 1000 and 10^6 cells/mL, respectively. Bioaerosol particles could be broken down into smaller pieces during the sampling process, which affects the results of subsequent analysis by culture- or fluorescence-based methods. We considered this effect on our LSPR sensor by treating *E. coli* samples with sonication.[47] The intact *E. coli* structure was broken down into small fragments by using high-frequency sound (35 kHz). As shown in Figure S4, the *E. coli* samples before and after the treatment yielded similar response levels at 0.2876 and 0.2939 rad, respectively. The results demonstrated that the response of our SEF−AuNIs sensor corresponded to the total amount of the bioaerosols, and the impact of bioaerosol breakdown was negligible. The regression relationship was further studied by testing the SEF−AuNIs sensors with eight different *E. coli* samples, as shown in Figure 2c. These responses indicated a positive correlation between the captured *E. coli* and LSPR responses. The linear-regression fitting was also applied in the range from 10 to 10^5 cells/mL, as shown in the inset of Figure 2c, and the regression relationship was found to be $y = 0.4024 \times x - 0.1994$ (with R^2 0.9404). The LOD of *E. coli* was found to be 0.5119 cells/mL (details in the Supporting Information), and the reliable dynamic range was from 10 to 10^5 cells/mL. The sensing characteristics of the SEF−AuNI sensors were further investigated with *Bacillus subtilis*, a Gram-positive bacterium. Similarly, the LOD was found to be 1.69 cells/mL based on the regression curves of *B. subtilis* as shown in Figure S5. Compared with previous SPR bacteria-sensing platforms,[48,49] the SEF−AuNI sensors exhibited improved sensitivity because of the tailored nanostructure and advanced phase-modulation methods.

The sensing specificity of the SEF−AuNIs sensors was tested by aniline and ammonium nitrite, which represented the airborne organic amine and inorganic ammonium, respectively. The NH_x components in these two chemicals were suspected to negatively impact bioaerosol detection as they might react with the functionalized succinimidyl ester. Atmospheric ammonium (AAM) has been recognized as one of the air pollutants which could form ammonium-containing aerosols. The agricultural activities, industrial, and traffic emissions are

https://dx.doi.org/10.1021/acs.est.9b05184
Environ. Sci. Technol. XXXX, XXX, XXX−XXX

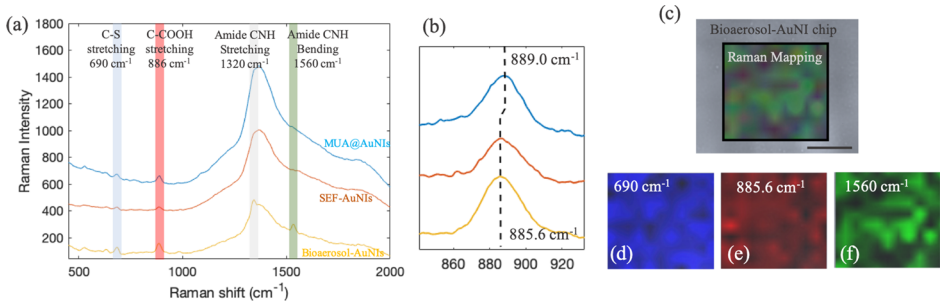

Figure 3. (a) SERS spectra of SEF−AuNI sensors showed the characteristic peaks from 11-MUA, EDC/NHS activation, and bioaerosols, (b) C−COOH stretching signal shifts due to the surface activation. (c) SEF−AuNI image and pseudo SERS mapping by combining three characteristic scans at (d) 690, (e) 885.6, and (f) 1560 cm^{-1}. The scale bar is 10 μm.

the main ammonium sources.[50] To evaluate the influence of AAM, the SEF−AuNIs sensors were tested by seven different concentrations of ammonium ions, ranging from 10 ng/mL to 10 mg/mL (Figures 2d and S6). It was observed that the phase response proportionally increased with ammonium ion concentration until it reached saturation at 1 mg/mL (Figure 2d). Nonetheless, the phase response values were relatively low, and the maximum response saturated at about 0.45 rad. Similarly, the sensing selectivity toward the organic amine was also tested with 6 as-prepared aniline aqueous solutions from 10 ng/mL to 1 mg/mL. The aniline response saturated at approximately 0.1 mg/mL and the maximum response reached 0.51 rad (Figure 2e). It is noted that the RI changes of the bulk solution caused by concentrated aniline and ammonium might have also contributed to the phase shift. According to the literature,[50−53] the common concentration ranges of ammonium, aniline, and bioaerosols in a human settlement environment were estimated to be about 0.5−5 $\mu g/m^3$, 0.01−1 $\mu g/m^3$, and 10^3−10^6 cells/m^3, respectively. Here, we assume that the transfer efficiencies from the airborne state to liquid were the same toward these three compounds and the aerosols in 1 m^3 of air were transferred into 1 mL liquid buffer. Thus, the sensing responses were compared within the relative concentration ranges of 0.5−5 μg/mL, 0.01−1 μg/mL, and 10^3−10^6 cells/mL. Based on the regression relationships, the mean sensing responses of inorganic ammonium and organic amines within the common concentration ranges were found to be 0.144 and 0.134 rad, respectively. These two responses were significantly lower than the mean response at 1.41 rad when detecting *E. coli* (Figure 2f). Particularly, the phase responses of ammonium and aniline were just 10.2 and 9.5% of that of *E. coli*, respectively. Even in the environments with a low bioaerosol concentration at 10^3 cells/m^3, the bioaerosol-induced response of the SEF−AuNIs sensor was still significantly higher than those of disturbances such as ammonia and aniline. Moreover, we can control the dilution ratio to feed samples from heavily contaminated environments into the SEF−AuNIs. It is worth noting that LSPR-based SEF−AuNIs sensors detect the binding events by identifying the local RI changes. The bioaerosols, normally ranging from tens of nanometers to micrometers, could cause significantly higher local RI changes than the non-biological NH_x in the atmosphere. Our results further proved that the SEF−AuNIs can distinguish the airborne biological amine without being strongly disturbed by the nonbiological NH_x events. In fact, a high ammonia or aniline concentration may contribute to a false positive signal in some aggressive environments, including animal husbandry and NH_3-based fertilizer applications. Therefore, the proposed SEF−AuNIs are recommended for bioaerosol detection in normal living environments, while usage in an aggressive environment requires additional auxiliary units to reduce the level of disturbances. Moreover, the weak noncovalent interactions, including nonspecific hydrophilic adsorption and van der Waals bound particles can be eliminated by direct buffer flushing. Only the covalently bonded microorganisms can remain on the SEF−AuNI interfaces.

Interface Characterization by SERS. Even though the Raman scattering cross section is typically too small for direct measurement, the AuNI sensors with uniform particle distribution, high surface roughness, and local-field enhancement can be a good platform for the Raman study. SERS can directly provide fingerprint identification of immobilized ligands and the microscale distribution of the captured bioaerosols. As shown in Figure 3a, the SERS spectrum (with 600 g/mm grating) of MUA@AuNIs showed peaks at around 690 and 886 cm^{-1}, which were assigned to C−S and C−COOH stretching, respectively.[54] After surface activation, these two bands survived, but the C−COOH stretching peak slightly shifted from 889.0 to 885.6 cm^{-1} (Figure 3b). This can be explained by the carboxyl group activation and ester group formation. The SEF−AuNI sensor was subsequently used to detect the bioaerosols, and the signals of the amide CNH group appeared at 1320 cm^{-1} (amide CNH stretching) and 1560 cm^{-1} (amide CNH bending), as shown in Figure S7, which were in good agreement with previous data.[55] Moreover, here, we also conducted Raman investigation with a 300 g/mm grating and the result was given in Figure S8. The spectrum showed two weak peaks at 690 and 889 cm^{-1} for C−S and C−COOH, respectively, and a strong C−C peak at 1099 cm^{-1}. In order to better characterize the SEF−AuNI interface, three pseudo mappings at 690, 885.6, and 1560 cm^{-1}, representing the C−S stretching, C−COO^- stretching, and CNH bending were reconstructed, as shown in Figure 3c−f. In Figure 3c, a white-light microscopic image and multichannel scanning image are given. The pseudo-maps at 690 and 885.6 cm^{-1} proved that the surface-functionalized chemicals, that is, 11-MUA and EDC/NHS were uniformly immobilized on the AuNI surface, as shown in Figure 3d,e. The pseudo-mapping of 1560 cm^{-1} amide CNH which showed a granular distribution of bright green patches indicated that the bioaerosols were successfully captured by our SEF−AuNI sensors (Figure 3f). Moreover, the scanned bioaerosols also exhibited a unique SERS spectrum (Figure S9), which might be used for bioaerosol classification and further analysis. In comparison with other bioaerosol detection systems, the SEF−AuNIs

https://dx.doi.org/10.1021/acs.est.9b05184
Environ. Sci. Technol. XXXX, XXX, XXX−XXX

LSPR system could be a versatile bioaerosol analysis platform for both total bioaerosol concentration monitoring and SERS aerosol analysis.

Bioaerosol Detection from Real-World Environmental Samples. In order to evaluate the applicability of the SEF−AuNI sensors for total bioaerosol monitoring, environmental aerosol samples collected during January to December 2017 from three different cities in Switzerland were tested (Figure 4a). The monthly aerosol samples were tested offline,

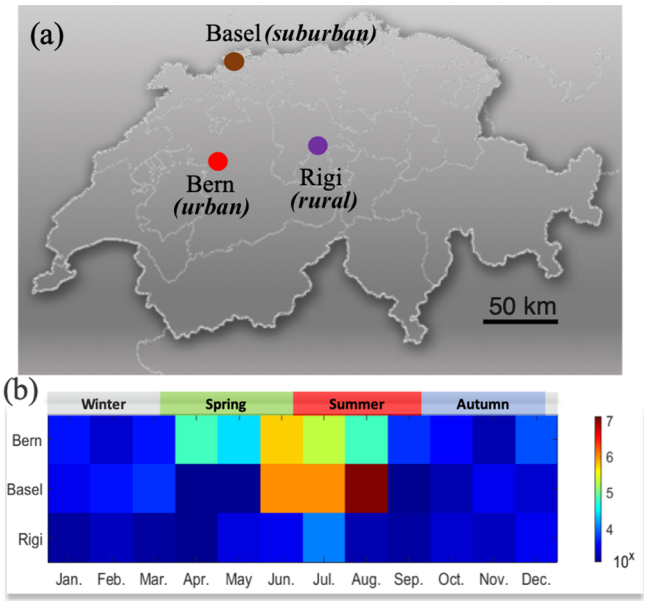

Figure 4. (a) Geographic locations of the three sampling cities. (b) Total bioaerosol concentrations of these three environmental scenarios were analyzed monthly with the proposed SEF−AuNI sensors.

and the corresponding sensorgrams are given in Figure 5. The mean value during the steady period of PBS buffer flushing was calculated. Subsequently, this mean response was applied in the regression equation (Figure 2c) to evaluate the bioaerosol concentration in each monthly sample. Although bioaerosols in the real-world environments are diverse and complex, the amino groups are common in these biocomponents and can be captured by SEF−AuNIs. Thus, the bioaerosol contents in these environmental samples can be calculated based on the calibrated regression of *E. coli* and identified as an *E. coli*-equivalent concentration, which is then further analyzed to illustrate the environmental characteristics of the sampling locations. It is worth noting that bioaerosols can be detected by forming a covalent bond between an amino group and a succinimidyl ester quickly; thus, this system can be used for analyzing samples in higher temporal resolution. As shown in Figure S10, two daily samples from February 1st, 2017 and August 1st, 2017 were measured with our proposed SEF−AuNI sensors. From the perspective of seasonal distribution as shown in Figure 4b, the bioaerosol contents in spring and summer, especially from June to August, were clearly higher than those in winter and autumn. In contrast, the bioaerosol contents from October to the coming March were all close to or below 10^4 cells/m^3 in these three tested environments. The peak bioaerosol contents all appeared in late spring or early summer. For the urban roadside environment in Bern, the maximum concentration of total bioaerosols was found to be

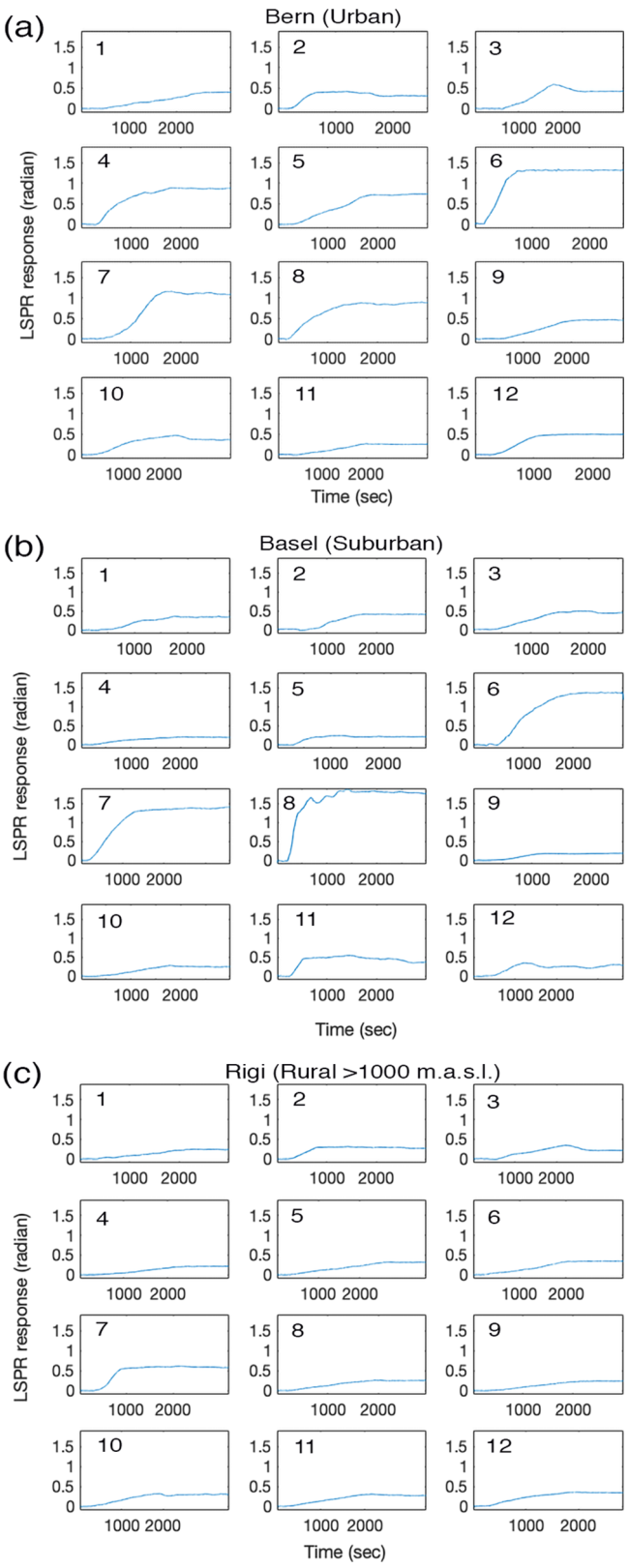

Figure 5. Real-time bioaerosols sensing toward the monthly samples from (a) Bern, (b) Basel, and (c) Rigi. The 12 subplots of each location indicate the monthly bioaerosol sensing responses from Jan 2017 to Dec 2017. The steady LSPR responses after buffer flushing were used to evaluate the bioaerosol concentrations.

about 6 × 10^5 cells/m^3 in June, while the suburban environment in Basel exhibited a high concentration from

https://dx.doi.org/10.1021/acs.est.9b05184
Environ. Sci. Technol. XXXX, XXX, XXX−XXX

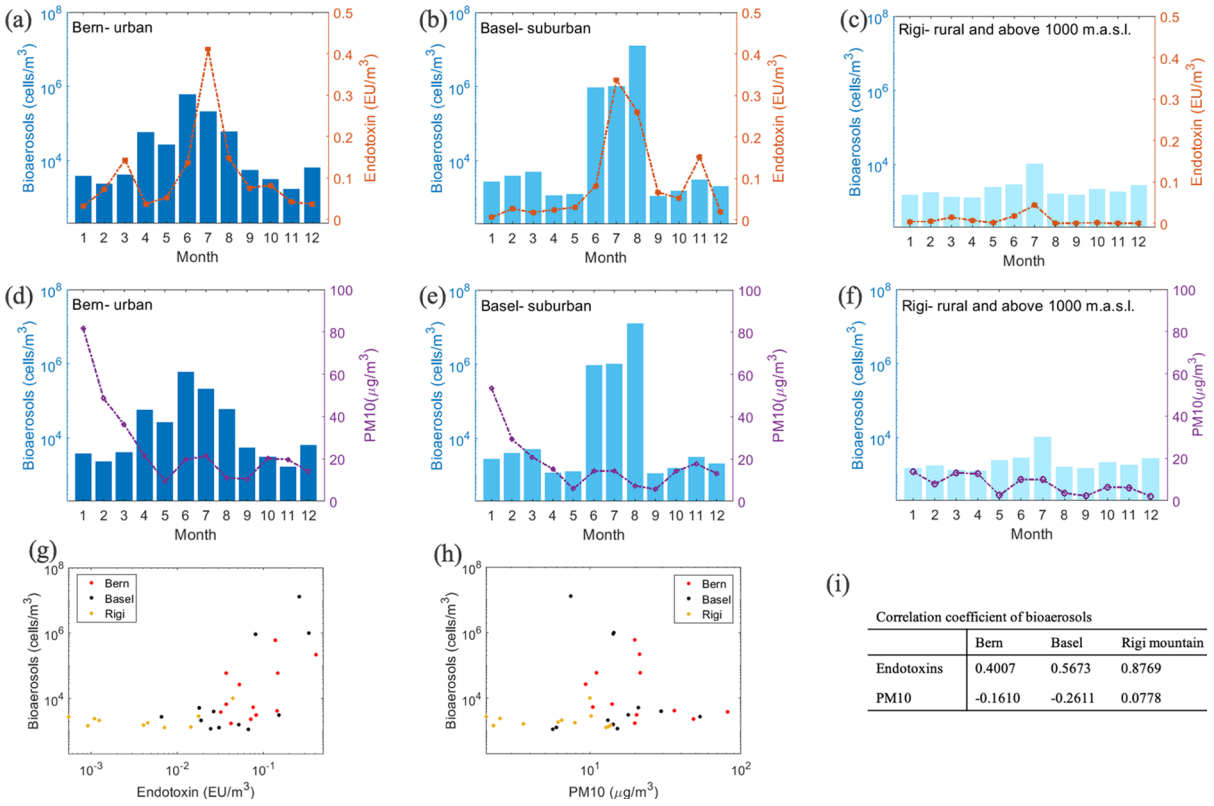

Figure 6. Comparison between monthly total bioaerosols and endotoxins at (a) Basel, (b) Bern, and (c) Rigi mountain. Comparison between monthly total bioaerosols and PM10 at (d) Basel, (e) Bern, and (f) Rigi mountain. Bioaerosol correlation with (g) endotoxin and (h) PM10 levels, and (i) the PCC for different environments.

June to August. The highest bioaerosol concentration was found in August reaching 1.28×10^7 cells/m^3. As a high-altitude and low-human-settlement region, Rigi mountain maintained the bioaerosol concentration within a low-level ranging from 1.3×10^3 cells/m^3 in April to 1.0×10^4 cells/m^3 in July. Previous studies indicated that warmer climate can directly promote the replication and growth of majority of viable bioaerosols, extend the bioaerosol lifetime, and increase the metabolic activity of living bioaerosols.[56,57] Meanwhile, the warmer climate can increase the water saturation vapor pressure. Thus, the high moisture content can protect the bioaerosols from desiccation stress.[58] In contrast, the relatively low annual temperature (mean at 7.5 °C) and high wind speed at the high-altitude environment of Rigi mountain could significantly depress the metabolism and physiological activity.

The environmental samples were also analyzed in terms of endotoxin and PM10 (PM with a diameter of 10 μm or less), to understand the aerosol contents and further verify the SEF−AuNIs sensing performance. Endotoxins are LPS of the Gram-negative bacteria wall, which consists of lipid, O-antigen, and polysaccharide chain.[59] Endotoxins have been considered as one of the main factors contributing to occupational lung disease and multiorgan injuries.[8,60] PM10 can be brought into air by various natural and human activities, subsequently suspended over long time to travel long distances in atmosphere.[61] The correlation among bioaerosols, endotoxins, and PM10 concentrations was analyzed as shown in Figure 6a−f. For endotoxins, the concentration from June to August was significantly higher than that of other months in these three reported environmental scenarios. This result was consistent with the bioaerosol level measured by the SEF−AuNI sensors. In contrast, the PM10 concentration during the cold season was found to be substantially higher than other months in both urban and suburban regions, which was attributed to anthropogenic sources such as wood-burning and fuel combustion.[62] For the rural and high-altitude environment (i.e., Rigi mountain), the concentration of PM10 in the cold season was not obviously higher. The relationship among bioaerosols, endotoxins, and PM10 was further evaluated with Pearson's correlation coefficient (PCC), as shown in Figure 6i. The bioaerosol concentration measured by the SEF−AuNIs sensors showed positive correlations with ambient endotoxin concentration in all three environments, that is, $R_{Bern} = 0.40$, $R_{Basel} = 0.57$, and $R_{Rigi} = 0.88$. The seasonal variation of temperature and RH affected the total bioaerosol concentration; the Gram-negative bacteria as part of the total bioaerosols followed a similar trend which was reflected in the endotoxin seasonal change. Therefore, the positive correlation between the measurements by the SEF−AuNIs and endotoxin tests was obtained. It is worth noting that the LPS is the major component of the outer membrane of Gram-negative bacteria, which can be a reliable indicator for pulmonary distress or impairment. However, the endotoxin level cannot represent all airborne biological toxins in the air. In contrast, the proposed SEF−AuNIs can provide a more comprehensive indicator to the total airborne biological particles. As shown in Figure 6h,i, the PCCs between PM10 and bioaerosols were weakly negative (i.e., −0.161, −0.261 in Bern and Basel, respectively) or close to zero (i.e., 0.078 in Rigi rural region). These coefficients indicated that PM10 and bioaerosols were not clearly correlated, and the proposed SEF−AuNIs were able to obtain the bioaerosols in a monthly

https://dx.doi.org/10.1021/acs.est.9b05184
Environ. Sci. Technol. XXXX, XXX, XXX−XXX

trend even under the interference of PM. An interesting feature in detecting the winter samples was scrutinized as shown in Figure S11. The environmental aerosol samples with high PM contents showed obvious dissociation when flushed with PBS buffer. This dissociation was attributed to the nonspecific binding of PM near the SEF−AuNI interface. These noncovalent bonds were relatively weak and unstable; therefore, it is easy to be removed by flushing. For the environmental aerosol sample from June, there was no observable dissociation after PBS flushing, as the covalently captured bioaerosols had good stability on the SEF−AuNI interface. According to the AFM images in Figure S2a, there were approximately 264 AuNIs per square micrometer. Thus, the total AuNI number in the sensing interface (with an area of 28.64 mm^2) was estimated to be 7.56×10^9. These AuNIs were covered by smaller SEF ligands, so the total amount of active bioaerosol receptors was at least four orders higher than that of PM particles in the test sample. Even with the presence of substantial PM, the SEF−AuNI system was able to reliably detect bioaerosol concentrations based on surface binding and buffer rinses. Moreover, the bioaerosol mass and number fractions in PM samples from different environments were also calculated based on the SEF−AuNI sensing results and PM10 results, as shown in Figures S12−S15. Higher bioaerosol mass fractions in warm seasons were found in urban (Bern) and suburban areas (Basel), and the highest bioaerosol mass fraction in PM samples can reach 47.7% in the suburban area, as shown in Figure S13. According to the literature, measurements in different countries, for example, Ireland, Germany, China, and Spain reported that the bioaerosol mass or number fractions ranged between 0.1 and 50%.[63−66] For instance, the bioaerosol mass fraction in Huangshi City, China, ranged from 1.5 to 15% of the PM10.[63] However, the bioaerosol number fraction measured by WIBS in Spain ranged from 2 to 10% of the total particle population.[64] Thus, the bioaerosol mass fractions revealed by SEF−AuNI sensors were within a reasonable range from 0.01 to 47.7%. In contrast, the number-based bioaerosol fractions were relatively low. The annual average bioaerosol number fractions in Bern, Basel, and Rigi were all lower than 0.1% of the PM sample. Based on the LSPR principle, the SEF−AuNI response was generally proportional to the mass of captured bioaerosols. Figure S4 showed that the sensor signals correlated well with the total mass of the bacteria instead of the number of fragmented pieces of the bacteria. Thus, the proposed SEF−AuNI system is recommended to be used in the mass-fraction evaluation.

Environmental Implications. Accurate and fast detection of total bioaerosols in different environments is an important task for safeguarding against biological threats and broadening the pool of bioaerosol knowledge. Currently, offline analysis of specific bioaerosol species mainly relies on PCR techniques, while the fluorescence method is used for online quantification.[20,21,67] As summarized in Table S2, quantitative investigations of airborne bacteria or antibiotic resistance genes provided abundant information of their distributions, behaviors, and impacts. Because of the high diversity of bioaerosols and their potential toxicity, detection of total bioaerosols in different environmental settings over annual cycles can significantly contribute to our understating of the link between bioaerosols and human health. For the first time, we developed an innovative LSPR sensing system based on SEF−AuNIs for total bioaerosol detection. The proposed system was employed to detect total bioaerosols by covalently capturing the biological events with the activated succinimidyl-ester groups. The SEF−AuNI system was calibrated with *E. coli* (and alternatively *B. subtilis*); thus, the detected bioaerosols can be quantified as an *E. coli*-equivalent concentration based on the regression. In the test of real-world PM samples from three different environmental scenarios, the SEF−AuNI sensing platform was able to reveal the monthly trend of total bioaerosols without being interfered by other airborne PMs. The LSPR sensing results of urban, suburban, and rural environments of Switzerland indicated relatively high bioaerosol contents during the hot season. The seasonal variation of bioaerosols was reasonably correlated with endotoxins but not with PM10. Moreover, the proposed SEF−AuNIs system was used to evaluate the mass fraction in the collected PM samples. Being inspired by the current work, we believe that the SEF−AuNI-based LSPR sensing system offers a versatile bioaerosol analysis platform that goes beyond the current approach of single analyte detection. The proposed SEF−AuNIs sensing system can be used for both online bioaerosol detection by combining with a suitable sampling system and offline analysis for bioaerosol characterization and identification. Specifically, the current total bioaerosol detection system can be used as a trigger to determine when to employ further SERS or immuno-LSPR analyses for the identification of specific bioaerosol. Achieving such a goal in the future will be essential to combat the airborne biological threats and eventually promote the public health.

■ ASSOCIATED CONTENT

Supporting Information

The Supporting Information is available free of charge at https://pubs.acs.org/doi/10.1021/acs.est.9b05184.

Additional details on the chemical information, AuNI characterization and LSPR phase modulation, *B. subtilis* detection, SERS investigation, daily environmental samples detections, and bioaerosol mass- and number-fractions in PM10 (PDF)

■ AUTHOR INFORMATION

Corresponding Author

Jing Wang − *ETH Zürich, Zürich, Switzerland, and Empa, Swiss Federal Laboratories for Materials Science and Technology, Dübendorf, Switzerland;* orcid.org/0000-0003-2078-137X; Email: jing.wang@ifu.baug.ethz.ch

Other Authors

Guangyu Qiu − *ETH Zürich, Zürich, Switzerland, and Empa, Swiss Federal Laboratories for Materials Science and Technology, Dübendorf, Switzerland*

Yang Yue − *ETH Zürich, Zürich, Switzerland, and Empa, Swiss Federal Laboratories for Materials Science and Technology, Dübendorf, Switzerland*

Jiukai Tang − *ETH Zürich, Zürich, Switzerland, and Empa, Swiss Federal Laboratories for Materials Science and Technology, Dübendorf, Switzerland*

Yi-Bo Zhao − *ETH Zürich, Zürich, Switzerland, and Empa, Swiss Federal Laboratories for Materials Science and Technology, Dübendorf, Switzerland*

Complete contact information is available at: https://pubs.acs.org/10.1021/acs.est.9b05184

https://dx.doi.org/10.1021/acs.est.9b05184
Environ. Sci. Technol. XXXX, XXX, XXX−XXX

Author Contributions

G.Q. and J.W. conceived of the idea and designed works. G.Q. conducted the sensing experiments, data analysis, and manuscript preparation. Y.Y. prepared and analyzed the environmental samples. J.T. and Y.-B.Z. helped with the sample preparation and measurement. All of the authors have discussed the results and have given approval to the final version of the manuscript.

Notes

The authors declare no competing financial interest.

■ ACKNOWLEDGMENTS

The authors thank the support from members of the Center for Filtration Research: 3M Corporation, A.O. Smith Company, Applied Materials, Inc., BASF Corporation, Boeing Company, Corning Co., Ltd., China Yancheng Environmental Protection Science and Technology City, Cummins Filtration Inc., Donaldson Company, Inc., Entegris, Inc., Ford Motor Company, Guangxi Wat Yuan Filtration System Co., Ltd., MSP Corporation; Samsung Electronics Co., Ltd., Xinxiang Shengda Filtration Technology Co., Ltd., TSI Inc., W. L. Gore & Associates, Inc., Shigematsu Works Co., Ltd., Mott Corporation and the affiliate member National Institute for Occupational Safety and Health (NIOSH). We thank Dr. Christoph Hüglin at Empa for providing the real-world PM samples from NABEL.

■ REFERENCES

(1) Fröhlich-Nowoisky, J.; Kampf, C. J.; Weber, B.; Huffman, J. A.; Pöhlker, C.; Andreae, M. O.; Lang-Yona, N.; Burrows, S. M.; Gunthe, S. S.; Elbert, W.; Su, H.; Hoor, P.; Thines, E.; Hoffmann, T.; Després, V. R.; Pöschl, U. Bioaerosols in the Earth system: Climate, health, and ecosystem interactions. *Atmos. Res.* **2016**, *182*, 346−376.

(2) Griffiths, W. D.; Decosemo, G. A. L. The assessment of bioaerosols: A critical review. *J. Aerosol Sci.* **1994**, *25*, 1425−1458.

(3) Rösch, P.; Harz, M.; Peschke, K.-D.; Ronneberger, O.; Burkhardt, H.; Schüle, A.; Schmauz, G.; Lankers, M.; Hofer, S.; Thiele, H.; Motzkus, H.-W.; Popp, J. On-line monitoring and identification of bioaerosols. *Anal. Chem.* **2006**, *78*, 2163−2170.

(4) Yang, K.; Li, L.; Wang, Y.; Xue, S.; Han, Y.; Liu, J. Airborne bacteria in a wastewater treatment plant: Emission characterization, source analysis and health risk assessment. *Water Res.* **2019**, *149*, 596−606.

(5) Li, J.; Chen, H.; Li, X.; Wang, M.; Zhang, X.; Cao, J.; Shen, F.; Wu, Y.; Xu, S.; Fan, H.; Da, G.; Huang, R.-j.; Wang, J.; Chan, C. K.; De Jesus, A. L.; Morawska, L.; Yao, M. Differing toxicity of ambient particulate matter (PM) in global cities. *Atmos. Environ.* **2019**, *212*, 305−315.

(6) Li, J.; Cao, J.; Zhu, Y.-g.; Chen, Q.-l.; Shen, F.; Wu, Y.; Xu, S.; Fan, H.; Da, G.; Huang, R.-j.; Wang, J.; de Jesus, A. L.; Morawska, L.; Peccia, J.; Yao, M.; Yao, M. S. Global Survey of Antibiotic Resistance Genes in Air. *Environ. Sci. Technol.* **2018**, *52*, 10975−10984.

(7) Humbal, C.; Gautam, S.; Trivedi, U. A review on recent progress in observations, and health effects of bioaerosols. *Environ. Int.* **2018**, *118*, 189−193.

(8) Kim, K.-H.; Kabir, E.; Jahan, S. A. Airborne bioaerosols and their impact on human health. *J. Environ. Sci.* **2018**, *67*, 23−35.

(9) Lacey, J.; Dutkiewicz, J. Bioaerosols and occupational lung disease. *J. Aerosol Sci.* **1994**, *25*, 1371−1404.

(10) Kallawicha, K.; Chuang, Y.-C.; Lung, S.-C. C.; Han, B.-C.; Ting, Y.-F.; Chao, H. J. Exposure to ambient bioaerosols is associated with allergic skin diseases in Greater Taipei residents. *Environ. Pollut.* **2016**, *216*, 845−850.

(11) Douwes, J.; Thorne, P.; Pearce, N.; Heederik, D. Bioaerosol health effects and exposure assessment: progress and prospects. *Ann. Occup. Hyg.* **2003**, *47*, 187−200.

(12) Kwon, K.; Park, J.-W.; Hyun, K.-A.; Kwak, B. S.; Yong, D. E.; Hwang, J.; Jung, H.-I. Continuous adsorption and photothermal lysis of airborne bacteria using a gold-nanoparticle-embedded-geometrically activated surface interaction (gold-GASI) chip. *Sens. Actuators, B* **2017**, *248*, 580−588.

(13) Damit, B. Droplet-based microfluidics detector for bioaerosol detection. *Aerosol Sci. Technol.* **2017**, *51*, 488−500.

(14) Jiang, X.; Jing, W.; Zheng, L.; Liu, S.; Wu, W.; Sui, G. A continuous-flow high-throughput microfluidic device for airborne bacteria PCR detection. *Lab Chip* **2014**, *14*, 671−676.

(15) Alex Huffman, J.; Perring, A. E.; Savage, N. J.; Clot, B.; Crouzy, B.; Tummon, F.; Shoshanim, O.; Damit, B.; Schneider, J.; Sivaprakasam, V.; Zawadowicz, M. A.; Crawford, I.; Gallagher, M.; Topping, D.; Doughty, D. C.; Hill, S. C.; Pan, Y. Real-time sensing of bioaerosols: Review and current perspectives. *Aerosol Sci. Technol.* **2019**, 1−56. , (just-accepted)

(16) Stetzenbach, L. D.; Buttner, M. P.; Cruz, P. Detection and enumeration of airborne biocontaminants. *Curr. Opin. Biotechnol.* **2004**, *15*, 170−174.

(17) Blais-Lecours, P.; Perrott, P.; Duchaine, C. Non-culturable bioaerosols in indoor settings: Impact on health and molecular approaches for detection. *Atmos. Environ.* **2015**, *110*, 45−53.

(18) Mbareche, H.; Brisebois, E.; Veillette, M.; Duchaine, C. Bioaerosol sampling and detection methods based on molecular approaches: No pain no gain. *Sci. Total Environ.* **2017**, *599*−*600*, 2095−2104.

(19) Yoo, K.; Lee, T. K.; Choi, E. J.; Yang, J.; Shukla, S. K.; Hwang, S.-i.; Park, J. Molecular approaches for the detection and monitoring of microbial communities in bioaerosols: A review. *J. Environ. Sci.* **2017**, *51*, 234−247.

(20) Xie, J.; Jin, L.; He, T.; Chen, B.; Luo, X.; Feng, B.; Huang, W.; Li, J.; Fu, P.; Li, X. Bacteria and Antibiotic Resistance Genes (ARGs) in PM2.5 from China: Implications for Human Exposure. *Environ. Sci. Technol.* **2018**, *53*, 963−972.

(21) Xie, J.; Jin, L.; Luo, X.; Zhao, Z.; Li, X. Seasonal Disparities in Airborne Bacteria and Associated Antibiotic Resistance Genes in PM2.5 between Urban and Rural Sites. *Environ. Sci. Technol. Lett.* **2018**, *5*, 74−79.

(22) Posada-Cespedes, S.; Seifert, D.; Beerenwinkel, N. Recent advances in inferring viral diversity from high-throughput sequencing data. *Virus Res.* **2017**, *239*, 17−32.

(23) Sivaprakasam, V.; Huston, A. L.; Scotto, C.; Eversole, J. D. Multiple UV wavelength excitation and fluorescence of bioaerosols. *Opt. Express* **2004**, *12*, 4457−4466.

(24) Swanson, B. E.; Huffman, J. A. Development and characterization of an inexpensive single-particle fluorescence spectrometer for bioaerosol monitoring. *Opt. Express* **2018**, *26*, 3646−3660.

(25) Primmerman, C. A. Detection of biological agents. *Linc. Lab. J.* **2000**, *12*, 3−32.

(26) Crouzy, B.; Stella, M.; Konzelmann, T.; Calpini, B.; Clot, B. All-optical automatic pollen identification: Towards an operational system. *Atmos. Environ.* **2016**, *140*, 202−212.

(27) Šaulienė, I.; Šukienė, L.; Daunys, G.; Valiulis, G.; Vaitkevicius, L.; Matavulj, P.; Brdar, S.; Panic, M.; Sikoparija, B.; Clot, B.; Crouzy, B.; Sofiev, M. Automatic pollen recognition with the Rapid-E particle counter: the first-level procedure, experience and next steps. *Atmos. Meas. Tech.* **2019**, *12*, 3435−3452.

(28) Sauvageat, E.; Zeder, Y.; Auderset, K.; Calpini, B.; Clot, B.; Crouzy, B.; Konzelmann, T.; Lieberherr, G.; Tummon, F.; Vasilatou, K. Real-time pollen monitoring using digital holography. *Atmos. Meas. Tech. Discuss.* **2019**, DOI: 10.5194/amt-2019-427.

(29) Sivakumar, P.; Fernández-Bravo, A.; Taleh, L.; Biddle, J. F.; Melikechi, N. Detection and classification of live and dead Escherichia coli by laser-induced breakdown spectroscopy. *Astrobiology* **2015**, *15*, 144−153.

(30) Dixon, P. B.; Hahn, D. W. Feasibility of detection and identification of individual bioaerosols using laser-induced breakdown spectroscopy. *Anal. Chem.* **2005**, *77*, 631−638.

https://dx.doi.org/10.1021/acs.est.9b05184
Environ. Sci. Technol. XXXX, XXX, XXX−XXX

(31) Leone, N.; Descroix, D.; Mohammed, S. Bioaerosol Detection with Atomic Emission Spectroscopy. In *Bioaerosol Detection Technologies*; Jonsson, P., Olofsson, G., Tjarnhage, T., Eds., 2014; pp 143−167.
(32) Hutter, E.; Fendler, J. H. Exploitation of localized surface plasmon resonance. *Adv. Mater.* **2004**, *16*, 1685−1706.
(33) Willets, K. A.; Van Duyne, R. P. Localized surface plasmon resonance spectroscopy and sensing. *Annu. Rev. Phys. Chem.* **2007**, *58*, 267−297.
(34) Usachev, E. V.; Usacheva, O. V.; Agranovski, I. E. Surface plasmon resonance-based real-time bioaerosol detection. *J. Appl. Microbiol.* **2013**, *115*, 766−773.
(35) Adducci, B. A.; Gruszewski, H. A.; Khatibi, P. A.; Schmale, D. G., III Differential detection of a surrogate biological threat agent (Bacillus globigii) with a portable surface plasmon resonance biosensor. *Biosens. Bioelectron.* **2016**, *78*, 160−166.
(36) Usachev, E. V.; Tam, A. M.; Usacheva, O. V.; Agranovski, I. E. The sensitivity of surface plasmon resonance based viral aerosol detection. *J. Aerosol Sci.* **2014**, *76*, 39−47.
(37) Usachev, E. V.; Agranovski, E.; Usacheva, O. V.; Agranovski, I. E. Multiplexed Surface Plasmon Resonance based real time viral aerosol detection. *J. Aerosol Sci.* **2015**, *90*, 136−143.
(38) Eduard, W.; Heederik, D.; Duchaine, C.; Green, B. J. Bioaerosol exposure assessment in the workplace: the past, present and recent advances. *Journal of environmental monitoring* **2012**, *14*, 334−339.
(39) Qiu, G.; Ng, S. P.; Wu, L. C.-M. Dielectric functionalization for differential phase detecting localized surface plasmon resonance biosensor. *Sens. Actuators, B* **2016**, *234*, 247−254.
(40) Beachy, R. N.; Loesch-Fries, S.; Tumer, N. E. Coat Protein-Mediated Resistance Against Virus Infection. *Annu. Rev. Phytopathol.* **1990**, *28*, 451−472.
(41) Voulhoux, R.; Bos, M. P.; Geurtsen, J.; Mols, M.; Tommassen, J. Role of a highly conserved bacterial protein in outer membrane protein assembly. *Science* **2003**, *299*, 262−265.
(42) Howlett, B. J.; Knox, R. B.; Heslop-Harrison, J. Pollen-wall proteins: release of the allergen antigen E from intine and exine sites in pollen grains of ragweed and Cosmos. *J. Cell Sci.* **1973**, *13*, 603−619.
(43) Bowman, S. M.; Free, S. J. The structure and synthesis of the fungal cell wall. *Bioessays* **2006**, *28*, 799−808.
(44) Qiu, G.; Ng, S. P.; Wu, C. M. L. Differential phase-detecting localized surface plasmon resonance sensor with self-assembly gold nano-islands. *Opt. Lett.* **2015**, *40*, 1924−1927.
(45) Qiu, G.; Ng, S. P.; Wu, C.-M. L. Bimetallic Au-Ag alloy nanoislands for highly sensitive localized surface plasmon resonance biosensing. *Sens. Actuators, B* **2018**, *265*, 459−467.
(46) Deng, S.; Wang, P.; Yu, X. Phase-sensitive surface plasmon resonance sensors: Recent progress and future prospects. *Sensors* **2017**, *17*, 2819.
(47) Monsen, T.; Lovgren, E.; Widerstrom, M.; Wallinder, L. In Vitro Effect of Ultrasound on Bacteria and Suggested Protocol for Sonication and Diagnosis of Prosthetic Infections. *J. Clin. Microbiol.* **2009**, *47*, 2496−2501.
(48) Subramanian, P.; Barka-Bouaifel, F.; Bouckaert, J.; Yamakawa, N.; Boukherroub, R.; Szunerits, S. Graphene-coated surface plasmon resonance interfaces for studying the interactions between bacteria and surfaces. *ACS Appl. Mater. Interfaces* **2014**, *6*, 5422−5431.
(49) Yoo, S. M.; Kim, D.-K.; Lee, S. Y. Aptamer-functionalized localized surface plasmon resonance sensor for the multiplexed detection of different bacterial species. *Talanta* **2015**, *132*, 112−117.
(50) Paulot, F.; Jacob, D. J.; Pinder, R. W.; Bash, J. O.; Travis, K.; Henze, D. K. Ammonia emissions in the United States, European Union, and China derived by high-resolution inversion of ammonium wet deposition data: Interpretation with a new agricultural emissions inventory (MASAGE_NH3). *J. Geophys. Res.: Atmos.* **2014**, *119*, 4343−4364.
(51) Asman, W. A. H.; Janssen, A. J. A long-range transport model for ammonia and ammonium for Europe. *Atmos. Environ.* **1987**, *21*, 2099−2119.
(52) Palmiotto, G.; Pieraccini, G.; Moneti, G.; Dolara, P. Determination of the levels of aromatic amines in indoor and outdoor air in Italy. *Chemosphere* **2001**, *43*, 355−361.
(53) Akyüz, M. Simultaneous determination of aliphatic and aromatic amines in ambient air and airborne particulate matters by gas chromatography-mass spectrometry. *Atmos. Environ.* **2008**, *42*, 3809−3819.
(54) Marques, F. C.; Oliveira, G. P.; Teixeira, R. A. R.; Justo, R. M. S.; Neves, T. B. V.; Andrade, G. F. S. Characterization of 11-mercaptoundecanoic and 3-mercaptopropionic acids adsorbed on silver by surface-enhanced Raman scattering. *Vib. Spectrosc.* **2018**, *98*, 139−144.
(55) Martins, M. L.; Eckert, J.; Jacobsen, H.; dos Santos, E. C.; Ignazzi, R.; de Araujo, D. R.; Bellissent-Funel, M.-C.; Natali, F.; Marek Koza, M.; Matic, A.; de Paula, E.; Bordallo, H. N. Raman and Infrared spectroscopies and X-ray diffraction data on bupivacaine and ropivacaine complexed with 2-hydroxypropyl-β-cyclodextrin. *Data Brief* **2017**, *15*, 25−29.
(56) Chandra Mouli, P.; Mohan, S.; Reddy, S. Assessment of microbial(bacteria) Concentrations of ambient air at semi-arid urban region: Influence of meteorological factors. *Appl. Ecol. Environ. Res.* **2005**, *3*, 139−149.
(57) Jones, A. M.; Harrison, R. M. The effects of meteorological factors on atmospheric bioaerosol concentrations-a review. *Sci. Total Environ.* **2004**, *326*, 151−180.
(58) Begert, M.; Frei, C. Long-term area-mean temperature series for Switzerland-Combining homogenized station data and high resolution grid data. *Int. J. Climatol.* **2018**, *38*, 2792−2807.
(59) Yue, Y.; Chen, H.; Setyan, A.; Elser, M.; Dietrich, M.; Li, J.; Zhang, T.; Zhang, X.; Zheng, Y.; Wang, J.; Yao, M. Size-Resolved Endotoxin and Oxidative Potential of Ambient Particles in Beijing and Zürich. *Environ. Sci. Technol.* **2018**, *52*, 6816−6824.
(60) Khedher, S. B.; Neri, M.; Guida, F.; Matrat, M.; Cenée, S.; Sanchez, M.; Menvielle, G.; Molinié, F.; Luce, D.; Stücker, I. Occupational exposure to endotoxins and lung cancer risk: results of the ICARE Study. *Occup. Environ. Med.* **2017**, *74*, 667−679.
(61) Kim, K.-H.; Kabir, E.; Kabir, S. A review on the human health impact of airborne particulate matter. *Environ. Int.* **2015**, *74*, 136−143.
(62) Minguillón, M. C.; Querol, X.; Baltensperger, U.; Prévôt, A. S. H. Fine and coarse PM composition and sources in rural and urban sites in Switzerland: local or regional pollution? *Sci. Total Environ.* **2012**, *427*−*428*, 191−202.
(63) Liu, T.; Chen, L.-W. A.; Zhang, M.; Watson, J. G.; Chow, J. C.; Cao, J.; Chen, N.; Yao, R.; Xiao, W.; Chen, H.; Wang, W.; Zhang, J.; Zhan, C.; Liu, H.; Zheng, J. Bioaerosol Concentrations and Size Distributions during the Autumn and Winter Seasons in an Industrial City of Central China. *Aerosol Air Qual. Res.* **2019**, *19*, 1095−1104.
(64) Calvo, A. I.; Baumgardner, D.; Castro, A.; Fernández-González, D.; Vega-Maray, A. M.; Valencia-Barrera, R. M.; Oduber, F.; Blanco-Alegre, C.; Fraile, R. Daily behavior of urban Fluorescing Aerosol Particles in northwest Spain. *Atmos. Environ.* **2018**, *184*, 262−277.
(65) Kenny, C. M.; Jennings, S. G. Background bioaerosol measurements at Mace Head. *J. Aerosol Sci.* **1998**, *29*, S779−S780.
(66) Jaenicke, R. Abundance of cellular material and proteins in the atmosphere. *Science* **2005**, *308*, 73.
(67) Bowers, R. M.; Clements, N.; Emerson, J. B.; Wiedinmyer, C.; Hannigan, M. P.; Fierer, N. Seasonal variability in bacterial and fungal diversity of the near-surface atmosphere. *Environ. Sci. Technol.* **2013**, *47*, 12097−12106.

https://dx.doi.org/10.1021/acs.est.9b05184
Environ. Sci. Technol. XXXX, XXX, XXX−XXX